

Stone-Wales graphene: A two-dimensional carbon semimetal with magic stabilityHengChuang Yin,^{1,2,*} Xizhi Shi,^{1,2,*} Chaoyu He,^{1,2,†} Miguel Martinez-Canales,^{3,‡} Jin Li,^{1,2} Chris J. Pickard,^{4,5,§} Chao Tang,^{1,2} Tao Ouyang,^{1,2} Chunxiao Zhang,^{1,2} and Jianxin Zhong^{1,2}¹Hunan Key Laboratory for Micro-Nano Energy Materials and Devices, Xiangtan University, Hunan 411105, People's Republic of China²School of Physics and Optoelectronics, Xiangtan University, Xiangtan 411105, China³SUPA, School of Physics and Astronomy and CSEC, University of Edinburgh, Peter Guthrie Tait Road, Edinburgh EH9 3FD, United Kingdom⁴Department of Materials Science and Metallurgy, University of Cambridge, 27 Charles Babbage Road, Cambridge CB3 0FS, United Kingdom⁵Advanced Institute for Materials Research, Tohoku University 2-1-1 Katahira, Aoba, Sendai 980-8577, Japan

(Received 8 August 2018; published 22 January 2019)

A two-dimensional carbon allotrope, Stone-Wales graphene, is identified in stochastic group and graph constrained searches and systematically investigated by first-principles calculations. Stone-Wales graphene consists of well-arranged Stone-Wales defects, and it can be constructed through a 90° bond rotation in a $\sqrt{8} \times \sqrt{8}$ supercell of graphene. Its calculated energy relative to graphene, +149 meV/atom, makes it more stable than the most competitive previously suggested graphene allotropes. We find that Stone-Wales graphene (SW-graphene) based on a $\sqrt{8}$ supercell is more stable than those based on $\sqrt{9} \times \sqrt{9}$, $\sqrt{12} \times \sqrt{12}$, and $\sqrt{13} \times \sqrt{13}$ supercells, and is a “magic size” that can be further understood through a simple “energy splitting and inversion” model. The calculated vibrational properties and molecular dynamics of SW-graphene confirm that it is dynamically stable. The electronic structure shows SW-graphene is a semimetal with distorted, strongly anisotropic Dirac cones.

DOI: [10.1103/PhysRevB.99.041405](https://doi.org/10.1103/PhysRevB.99.041405)

Elemental carbon adopts many different allotropes, including the three-dimensional (3D) cubic diamond, hexagonal diamond and graphite, the two-dimensional (2D) graphene [1] and graphynes [2], the one-dimensional (1D) nanotubes [3], as well as the zero-dimensional (0D) fullerenes [4], due to its ability to hybridize in sp , sp^2 , and sp^3 . Low-dimensional carbon materials, such as graphene and nanotubes, have attracted much scientific interest in view of their novel electronic and mechanical properties [1,5,6]. In particular, graphene is a well-known Dirac-cone material that exhibits high carrier mobility [1,5,6] and the quantum Hall effect [5,7,8] due to its semimetallicity contributed from the active π electrons [8,9]. The successes of isolating graphene [1,10,11] from graphite have spurred many efforts in searching for other 2D carbon allotropes beyond graphene. Graphynes [12,13] are alternative ways to fill the 2D space with mixed sp - sp^2 carbon atoms. They contribute rich electronic properties, including semiconductors, semimetals, and metals. Although graphynes with sp -hybridized bonding are energetically less stable than the pure sp^2 -hybridized graphene, graphite, and nanotubes, there are a few graphynes that have been experimentally synthesized [2,14].

The honeycomblike graphene is not the only way to topologically fill 2D space with sp^2 hybridized carbon. Many

other hypothetical graphene allotropes have been previously proposed. For example, the pentaheptites (R_{57-1} and R_{57-2}) containing exclusively 5–7 rings proposed in 1996 [15] and 2000 [16,17], the Haeckelite sheets (H_{567} and O_{567}) proposed by Terrones [17], the low-energy ψ -graphene previously proposed by Csányi [18] and recently investigated by Li [19], the dimerites (dimerite I, II, and III with metallic property) and octites (metallic octite M_1 , M_2 , M_3 , and semiconducting octite SC) constructed through defect patterns [20–23], the biphenylene sheets (New-W and New-C) containing 4-6-8 rings [24,25], the T-graphene containing 4-8 rings [26–28], the PO-graphene containing 5-8 rings (OPG-L and OPG-Z) [29,30], the graphene superlattice structures (including pza- C_{10}) [31], the 187- C_{65} , 191- C_{63} , and 127- C_{41} sheets [32], the 5-6-8 rings of HOP-graphene [33], δ -graphene [34], and pentahexoctite [35], as well as the recently proposed phagraphene [36]. Most of these 2D carbon allotropes are more energetically stable than the experimentally viable graphynes [2,14] and C_{60} [4]. In particular, the most stable ψ -graphene [8] and phagraphene [36] possess energies just about 165 and 201 meV/atom higher, respectively, than that of graphene, and might be synthesized in future experiments.

Previously suggested 2D carbon allotropes, other than octite SC [23], have less than 20 atoms per cell. In this work, we have performed stochastic group and graph-constrained searches for 2D carbon allotropes with up to 24 atoms per unit cell. Graph-constrained searches have been performed using our recently developed RG² code [37]. Structural details, energetics, and properties have all been computed using density functional theory (DFT) and the PBE exchange-

*These authors contributed equally to this work.

†hechaoyu@xtu.edu.cn

‡miguel.martinez@ed.ac.uk

§cjp20@cam.ac.uk

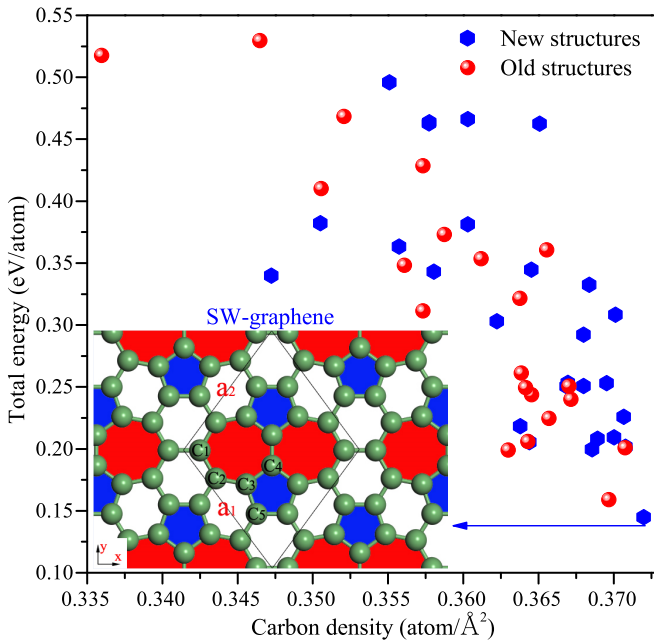


FIG. 1. Calculated energies (relative to graphene) and carbon densities of the new discovered (blue hexagon) and previously proposed (red balls) graphene allotropes with energy relative to graphene less than 550 meV per atom. Inset: The crystalline view of the most stable one (SW graphene) with symmetry of C_{mmm} , showing its topological pattern containing five-, six-, and sevenfold carbon rings.

correlation functional [38] as implemented in the Vienna *ab initio* simulation package (VASP) [39]. Carbon was modeled with a $2s^2 2p^2$ projector augmented wave potential [40,41] and the energy cutoff was set to be 500 eV. The Brillouin zone (BZ) sampling meshes were denser than 0.21 \AA^{-1} to ensure the convergence. The vibrational spectrum of Stone-Wales graphene was computed using the PHONOPY code [42].

Our RG² searches produced nearly all the previously proposed 2D carbon allotropes. It further identified 33 previously unreported competitive structures as shown in Fig. 1, including the most stable allotrope known to date. Its structure contains well-arranged Stone-Wales defects (SWD; 5577-ring segments) [43–45] on a $\sqrt{8}$ graphene supercell, and we call it Stone-Wales graphene (SW-graphene hereafter). SW-graphene, shown in Fig. 1, has 16 carbon atoms and one SWD in its primitive unit cell. The SWDs periodically connect to each other with sixfold carbon rings boundary. As indicated in Fig. 1, the primitive cell (with optimized lattice constants of $a = b = 6.683 \text{ \AA}$, $c = 12.00 \text{ \AA}$, and $\gamma = 105.779^\circ$) of SW-graphene contains five inequivalent carbon atoms C_1 , C_2 , C_3 , C_4 , and C_5 , located at positions $4h$ (0.09, 0.09, 0.5), $8q$ (0.299, 0.062, 0.5), $8q$ (0.497, 0.211, 0.5), $4j$ (0.564, 0.435, 0.5), and $4j$ (0.682, 0.143, 0.5), respectively. The bond lengths (1.378–1.458 \AA) and bond angles (106.11–133.95 $^\circ$) [46] in SW-graphene are very close to those in ideal graphene, which indicate that it should be a low-lying 2D carbon allotrope.

We calculated the energies of the newly discovered and previously proposed graphene allotropes [46]. Those with energy relative to graphene less than 550 meV/atom are shown in Fig. 1. The most stable three graphene allotropes

previously proposed, ψ -graphene [18,19], octite M_1 [22], and phagraphene [36], lie 159, 199, and 201 meV/atom above graphene, respectively. The relative energy of SW-graphene is +149 meV/atom, which indicates that it is energetically more favorable than either. We notice that the carbon density of SW-graphene (0.372 atom/\AA^2) is also comparable to that of graphene (0.379 atom/\AA^2), larger than all the previously proposed 2D carbons.

With its remarkable energetic stability, SW-graphene might be synthesized if it is dynamically stable. The phonon dispersion bands and phonon density of states of SW-graphene show no imaginary frequency mode in the whole Brillouin zone [46], indicating SW-graphene is dynamically stable. *Ab initio* NVT molecular dynamics on a 3×3 supercell and a time step of 1 fs confirm that SW-graphene is dynamically stable at 300 K for at least 5 ps. No structural changes occur, with the only distortion being thermal oscillations of atoms near their equilibrium positions (Fig. S3 in the Supplemental Material [46]). That is to say, SW-graphene should be stable at room temperature.

As discussed in previous literature concerning the synthesis of ψ -graphene [18] and phagraphene [36], defect topology [44,47,48] and molecular assembly [49,50] are two potential routes to synthesize SW-graphene. We notice that SW-graphene can be decomposed as ethylene and benzene (or cyclopentene and propylene) as indicated in Fig. S3. That is to say, catalyzer-associated assembly of ethylene and benzene (or cyclopentene and propylene) on a proper substrate could be a way to synthesize SW-graphene.

Most of the previously proposed graphene allotropes, such as ψ -graphene [18,19] and octite M_1 [22] are metallic. A few of them have been reported as semiconductors and semimetals, such as octite SC [23] and phagraphene [36]. Our calculations show that SW-graphene is a semimetal with distorted Dirac cones. There are two equivalent Dirac cones in its first Brillouin zone (BZ) as indicated in Fig. 2(a). The calculated band structure of SW-graphene along the pathway of $Y'-X-\Gamma-R-Y-\Gamma-S-X$ is shown in Fig. 2(b). A symmetry analysis shows that, along $Y'-\Gamma$, at least one band must cross the Fermi energy (D_6). We can see that there is a Dirac point located at the point (D_1) between R-Y. The calculated density of states at Fermi level is zero, which confirms that such a Dirac point is not formed by band folding. Figure 2(c) shows the energy difference between the highest valance band (HVB) and the lowest conduction band (LCB). We can see that there are six zero points (Dirac points) within that region. D_2 is equivalent to D_1 due to mirror symmetry along the y axis. D_6 (D_5) is equivalent to D_2 (D_1) via a reciprocal lattice vector shift of b_1 (negative b_2) as indicated in Fig. 2(a). D_4 and D_3 are equivalent to D_1 and D_2 , respectively, due to the mirror symmetry on the x axis.

To further understand the formation of the Dirac cones in SW-graphene, the band-decomposed charge density distributions of the four points (1,2,3,4) near the Dirac point D_6 are investigated. As shown in Fig. 2(d), we can see that the charge densities of points 1 and 4 are very similar to each other. Those for points 2 and 3 also appear in same distribution. This indicates that the Dirac points in SW-graphene are formed by band crossings similar to those in phagraphene [36].

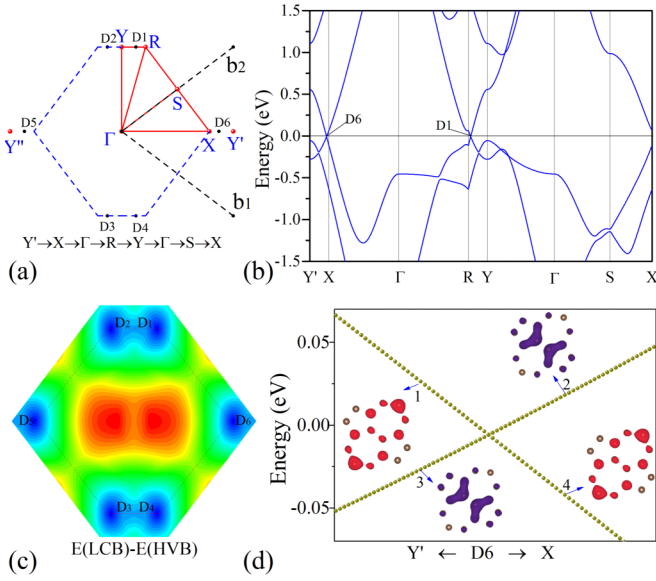


FIG. 2. The first Brillouin zone (BZ) (a), the band structures (b), the 2D color mapping of the energy differences between LCB and HVB (c), as well as the band decomposed charge density distributions of SW-graphene (d).

To show the conelike feature of these Dirac points, the 3D surface band structures of the HVB and LCB near D_6 are plotted. As shown in Fig. 3, the HVB and LCB cross each other at point D_6 and form a distorted Dirac cone with obvious anisotropy. Based on the calculated surface band structures, we then investigated the direction-dependent Fermi velocities of the fermions in cone D_6 as shown in Fig. 3. The corresponding Fermi velocities are given by $v_f = E(k)/\hbar|k|$. Our calculated Fermi velocities of phagraphene along the x , y , and $-y$ directions are 6.54×10^5 m/s, 6.34×10^5 m/s, and 4.17×10^5 m/s, respectively. The largest and smallest Fermi velocities in graphene are 8.26×10^5 and 7.74×10^5 m/s, respectively. These results are consistent with those reported before [36]. However, we find that the largest Fermi

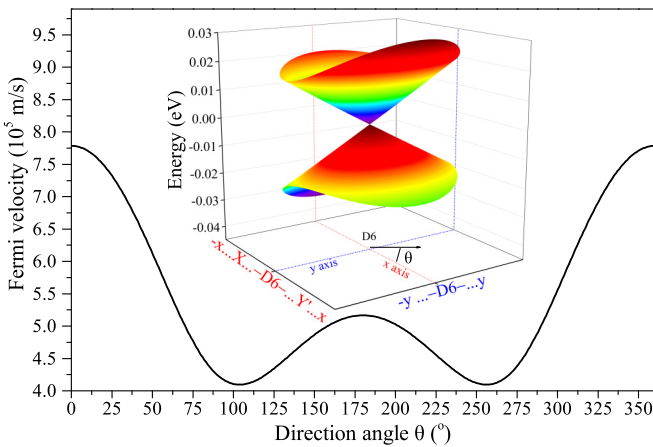


FIG. 3. The 3D plot of the Dirac cone formed by the highest valence band (HVB) and the lowest conduction band (LCB) in the vicinity of the Dirac point (D_6) and the corresponding direction-dependent Fermi velocities for Fermions in SW-graphene.

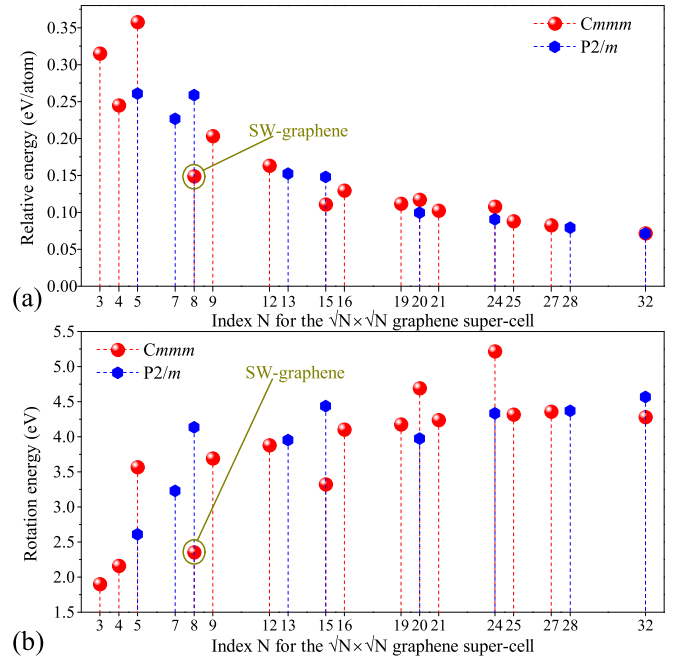


FIG. 4. Relative energies (a) and SWD rotation energies ($E_{\sqrt{N}} - NE_{\text{graphene}}$) (b) of $\sqrt{N} \times \sqrt{N}$ graphene supercells with a single SWD. SW-graphene corresponds to $N = 8$. Red balls denote structures that adopt $Cmmm$ symmetry; blue hexagons denote structures adopting $P2/m$ symmetry.

velocity in phagraphene is not the 6.54×10^5 m/s along the x direction. It is about 7.02×10^5 m/s along the $\pi/6$ direction, which was not reported in previous literature [36].

The result in Fig. 3 shows that the Fermi velocities of SW-graphene along the x ($\theta = 0^\circ$), $-x$ ($\theta = 180^\circ$), and y ($\theta = 90^\circ$) directions are 7.78×10^5 , 5.16×10^5 , and 4.25×10^5 m/s, respectively. Fermions in SW-graphene along the x direction possess the largest velocity of 7.78×10^5 m/s. Along the direction of $\theta \approx 7\pi/12$, the Fermi velocity (4.09×10^5 m/s) is the smallest. These results indicate that SW-graphene possesses anisotropic electronic properties similar to phagraphene [36], which are more obvious than those in graphene.

We have also computed the band structure using maximally localized Wannier functions using QUANTUM-ESPRESSO [51] and WANNIER90 [52]. Our starting guess has been p_z orbitals on each atom, sp^2 orbitals on alternating atoms where possible, and σ bonds on the remaining bonds. This replicates the DFT bands up to at least 4 eV above the Fermi energy [46]. Projecting into orbitals shows a picture similar to graphene: the low-lying bands come from sp^2 orbitals, while the bands near Fermi energy can be described by p_z interactions. The result of such a projection is shown in Fig. S6. This opens up the creation of an effective Hamiltonian for SW-graphene, but even a nearest-neighbor model has 15 symmetry-independent hopping parameters. The Berry phase around a Dirac cone takes a nontrivial value of π .

SW-graphene can be understood as a simple 90° carbon bond rotation [46]. However, we show now the stability of SW-graphene is not just the result of a single defect in a

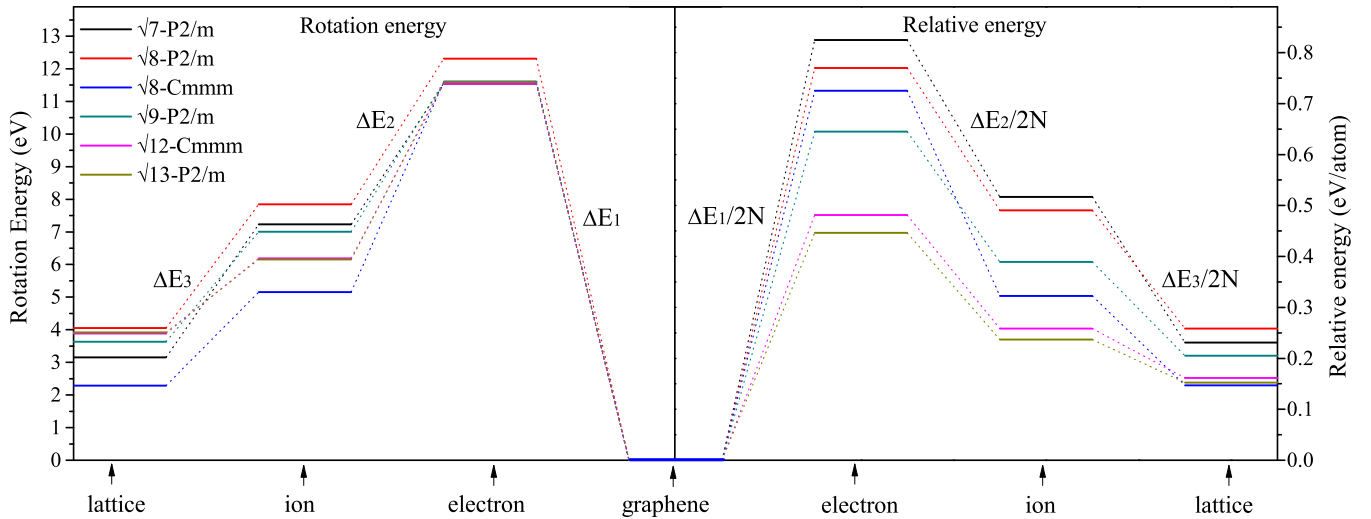


FIG. 5. Energy splitting and inversion model (left: rotation energies eV per cell; right: relative energies eV/atom relative to graphene) based on the comparison of energy changes between $\sqrt{7}$, $\sqrt{8}$ -Cmmm, $\sqrt{8}$ -P2/m, $\sqrt{9}$, $\sqrt{12}$, and $\sqrt{13}$ in three steps after bond rotation, namely, electronic minimization in fixed configuration (electron), ionic relaxation (ion), as well as full lattice and ionic relaxation (lattice).

supercell, and that SW-graphene is a structure in its own right. Figure 4(a) shows the energies of $\sqrt{N} \times \sqrt{N}$ graphene supercells with a single SWD. Larger cells are more stable, as expected, despite relaxation in smaller cells reducing a large fraction of the rotation energy penalty of a SWD. However, SW-graphene ($\sqrt{8}$ -Cmmm) is 50 meV/atom more stable than $N = 9$ and, unexpectedly, more stable than $N < 15$. The rotation energy in SW-graphene is almost as low as for the $N = 3, 4$ cases. This suggests $N = 8$ is a “magic size,” followed by two other magic sizes of $\sqrt{15}$ and $\sqrt{20}$.

A simple “energy splitting and inversion” model is used to understand the “magic stability” of SW-graphene as shown in Fig. 5. After bond rotation, we compare the energies and rotation energies of $\sqrt{7}$, $\sqrt{8}$ -Cmmm, $\sqrt{8}$ -P2/m, $\sqrt{9}$, $\sqrt{12}$, and $\sqrt{13}$ in three steps: electronic minimization in fixed configuration, ionic relaxation, as well as full lattice and ionic relaxation. In fixed configuration, other than an obvious energy penalty for $\sqrt{8}$ -P2/m, other candidates show roughly the same ΔE_1 . The averaged values $\Delta E_1/2N$ split or reverse the energy positions of $\sqrt{7}$, $\sqrt{8}$ -Cmmm, $\sqrt{8}$ -P2/m, $\sqrt{9}$, $\sqrt{12}$, and $\sqrt{13}$. After bond rotation, the defected atoms [53] in the system adjust their position to minimize the energy. With larger ratio of defected atoms, ionic and lattice relaxations release more energy ΔE_2 and ΔE_3 in small cells ($\sqrt{7}$, $\sqrt{8}$ -Cmmm, $\sqrt{8}$ -P2/m) than larger systems ($\sqrt{9}$, $\sqrt{12}$, and $\sqrt{13}$). The results in Fig. 5 show how $\sqrt{8}$ -Cmmm releases the largest amount of energy on ionic relaxation, which is eventually the cause of the stability of SW-graphene.

We finally check if Dirac cones are common features in the SW-graphene allotropes family [46]. SW-graphene allotropes $\sqrt{3}$, $\sqrt{4}$, $\sqrt{5}$ -Cmmm, $\sqrt{7}$, $\sqrt{9}$, $\sqrt{12}$, and $\sqrt{15}$ -Cmmm are all metallic. Those named as $\sqrt{5}$ -P2/m, $\sqrt{8}$ -P2/m, $\sqrt{13}$, $\sqrt{15}$ -P2/m, $\sqrt{19}$, $\sqrt{20}$ -Cmmm, $\sqrt{20}$ -P2/m, $\sqrt{21}$, $\sqrt{24}$ -P2/m, $\sqrt{28}$, and $\sqrt{32}$ -P2/m are semiconductors with direct or indirect band gaps. Only a few of

them are semimetals featuring Dirac cones: $\sqrt{8}$ -Cmmm (SW-graphene), $\sqrt{16}$, $\sqrt{24}$ -Cmmm, and $\sqrt{32}$ -Cmmm.

In summary, a 2D carbon allotrope is discovered using our recently developed RG² code. It is named SW-graphene in view of its structural feature consisting of the well-known Stone-Wales defects. The calculated total energy shows that SW-graphene is energetically more favorable than the previously proposed phagraphene and ψ -graphene. It is also confirmed to be a dynamically stable carbon phase according to its phonon dispersion and molecular dynamics. The calculated band structures show that SW-graphene is a semimetal with distorted Dirac cones, containing fermions with direction-dependent Fermi velocities. In view of its remarkable stability and novel properties, SW-graphene is a desirable target for future synthesis. A family of SW-graphene allotropes constructed through 90° rotation of carbon bonds in given $\sqrt{N} \times \sqrt{N}$ graphene supercells are investigated. We find that $\sqrt{8}$ -Cmmm SW-graphene is an interesting system with magic stability and not all the SW-graphene allotropes are semimetallic like $\sqrt{8}$ -Cmmm SW-graphene. The magic stability of $\sqrt{8}$ -Cmmm SW-graphene is further discussed based on a theoretical energy splitting and inversion model.

This work is supported by the National Natural Science Foundation of China (Grants No. 11704319 and No. 11404275), the National Basic Research Program of China (Grant No. 2015CB921103), the Natural Science Foundation of Hunan Province, China (Grant No. 2016JJ3118), and the Program for Changjiang Scholars and Innovative Research Team in University (Grant No. IRT_17R91). M.M.C. is grateful for computational support from the UK Materials and Molecular Modelling Hub, which is partially funded by EPSRC (EP/P020194), for which access was obtained via the UKCP consortium and funded by EPSRC Grant No. EP/P022561/1. C.J.P. is supported by the Royal Society through a Royal Society Wolfson Research Merit award.

- [1] K. S. Novoselov, A. K. Geim, S. V. Morozov, D. Jiang, Y. Zhang, S. V. Dubonos, I. V. Grigorieva, and A. A. Firsov, *Science* **306**, 666 (2004).
- [2] G. Li, Y. Li, H. Liu, Y. Guo, Y. Li, and D. Zhu, *Chem. Commun.* **46**, 3256 (2010).
- [3] S. Iijima, *Nature (London)* **354**, 56 (1991).
- [4] H. W. Kroto, J. R. Heath, S. C. O'Brien, R. F. Curl, and R. E. Smalley, *Nature (London)* **318**, 162 (1985).
- [5] Y. Zhang, Y.-W. Tan, H. L. Stormer, and P. Kim, *Nature (London)* **438**, 201 (2005).
- [6] K. I. Bolotin, F. Ghahari, M. D. Shulman, H. L. Stormer, and P. Kim, *Nature (London)* **462**, 196 (2009).
- [7] K. S. Novoselov, Z. Jiang, Y. Zhang, S. V. Morozov, H. L. Stormer, U. Zeitler, J. C. Maan, G. S. Boebinger, P. Kim, and A. K. Geim, *Science* **315**, 1379 (2007).
- [8] K. S. Novoselov, E. McCann, S. V. Morozov, V. I. Fal'ko, M. I. Katsnelson, U. Zeitler, D. Jiang, F. Schedin, and A. K. Geim, *Nat. Phys.* **2**, 177 (2006).
- [9] C. L. Kane and E. J. Mele, *Phys. Rev. Lett.* **95**, 226801 (2005).
- [10] K. S. Kim, Y. Zhao, H. Jang, S. Y. Lee, J. M. Kim, K. S. Kim, J. H. Ahn, P. Kim, J. Y. Choi, and B. H. Hong, *Nature (London)* **457**, 706 (2009).
- [11] Z. Z. Sun, Z. Yan, J. Yao, E. Beitler, Y. Zhu, and J. M. Tour, *Nature (London)* **468**, 549 (2010).
- [12] R. H. Baughman and H. Eckhardt, *J. Chem. Phys.* **87**, 6687 (1987).
- [13] N. Narita, S. Nagai, S. G. Suzuki, and K. J. Nakao, *Phys. Rev. B* **58**, 11009 (1998).
- [14] R. Matsuoka, R. Sakamoto, K. Hoshiko, S. Sasaki, H. Masunaga, K. Nagashio, and H. Nishihara, *J. Am. Chem. Soc.* **139**, 3145 (2017).
- [15] V. H. Crespi, L. X. Benedict, M. L. Cohen, and S. G. Louie, *Phys. Rev. B* **53**, R13303(R) (1996).
- [16] M. Deza, P. W. Fowler, M. Shtogrin, and K. Vietze, *J. Chem. Inf. Comput. Sci.* **40**, 1325 (2000).
- [17] H. Terrones, M. Terrones, E. Hernández, N. Grobert, J.-C. Charlier, and P. M. Ajayan, *Phys. Rev. Lett.* **84**, 1716 (2000).
- [18] G. Csányi, C. J. Pickard, B. D. Simons, and R. J. Needs, *Phys. Rev. B* **75**, 085432 (2007).
- [19] X. Y. Li, Q. Wang, and P. Jena, *J. Phys. Chem. Lett.* **8**, 3234 (2017).
- [20] M. T. Lusk and L. D. Carr, *Phys. Rev. Lett.* **100**, 175503 (2008).
- [21] M. T. Lusk and L. D. Carr, *Carbon* **47**, 2226 (2009).
- [22] D. J. Appelhans, L. D. Carr, and M. T. Lusk, *New J. Phys.* **12**, 125006 (2010).
- [23] D. J. Appelhans, Z. B. Lin, and M. T. Lusk, *Phys. Rev. B* **82**, 073410 (2010).
- [24] M. A. Hudspeth, B. W. Whitman, V. Barone, and J. E. Peralta, *ACS Nano* **4**, 4565 (2010).
- [25] X. Q. Wang, H. D. Li, and J. T. Wang, *Phys. Chem. Chem. Phys.* **15**, 2024 (2013).
- [26] J. Nisar, X. Jiang, B. Pathak, J. J. Zhao, T. W. Kang, and R. Ahuja, *Nanotechnology* **23**, 385704 (2012).
- [27] X. Q. Wang, H. D. Li, and J. T. Wang, *Phys. Chem. Chem. Phys.* **14**, 11107 (2012).
- [28] Y. Liu, G. Wang, Q. S. Huang, L. W. Guo, and X. L. Chen, *Phys. Rev. Lett.* **108**, 225505 (2012).
- [29] C. P. Tang and S. J. Xiong, *AIP Adv.* **2**, 042147 (2012).
- [30] C. Su, H. Jiang, and J. Feng, *Phys. Rev. B* **87**, 075453 (2013).
- [31] X. G. Luo, L. M. Liu, Z. P. Hu, W. H. Wang, W. X. Song, F. F. Li, S. J. Zhao, H. Liu, H. T. Wang, and Y. J. Tian, *J. Phys. Chem. Lett.* **3**, 3373 (2012).
- [32] H. G. Lu and S. D. Li, *J. Mater. Chem. C* **1**, 3677 (2013).
- [33] B. Mandal, S. Sarkar, A. Pramanik, and P. Sarkar, *Phys. Chem. Chem. Phys.* **15**, 21001 (2013).
- [34] X. Y. Fan, J. Li, and G. Chen, *RSC Adv.* **7**, 17417 (2017).
- [35] B. R. Sharma, A. Manianath, and A. K. Singh, *Sci. Rep.* **4**, 7164 (2014).
- [36] Z. H. Wang, X. F. Zhou, X. M. Zhang, Q. Zhu, H. F. Dong, M. W. Zhao, and A. R. Oganov, *Nano Lett.* **15**, 6182 (2015).
- [37] X. Z. Shi, C. Y. He, C. J. Pickard, C. Tang, and J. X. Zhong, *Phys. Rev. B* **97**, 014104 (2018).
- [38] J. P. Perdew, K. Burke, and M. Ernzerhof, *Phys. Rev. Lett.* **77**, 3865 (1996).
- [39] G. Kresse and J. Furthmüller, *Phys. Rev. B* **54**, 11169 (1996).
- [40] P. E. Blöchl, *Phys. Rev. B* **50**, 17953 (1994).
- [41] G. Kresse and D. Joubert, *Phys. Rev. B* **59**, 1758 (1999).
- [42] Phonopy, <http://atztogo.github.io/phonopy/>.
- [43] A. J. Stone and D. J. Wales, *Chem. Phys. Lett.* **128**, 501 (1986).
- [44] J. Kotakoski, A. V. Krasheninnikov, U. Kaiser, and J. C. Meyer, *Phys. Rev. Lett.* **106**, 105505 (2011).
- [45] J. Ma, D. Alfe, A. Michaelides, and E. G. Wang, *Phys. Rev. B* **80**, 033407 (2009).
- [46] See Supplemental Material at <http://link.aps.org/supplemental/10.1103/PhysRevB.99.041405> for additional discussions about structures, stabilities and electronic properties.
- [47] G. Schusteritsch and C. J. Pickard, *Phys. Rev. B* **90**, 035424 (2014).
- [48] J. Lahiri, Y. Lin, P. Bozkurt, I. I. Oleynik, and M. Batzill, *Nat. Nanotechnol.* **5**, 326 (2010).
- [49] J. V. Barth, G. Costantini, and K. Kern, *Nature (London)* **437**, 671 (2005).
- [50] L. Grill, M. Dyer, L. Lafferentz, M. Persson, M. V. Peters, and S. Hecht, *Nat. Nanotechnol.* **2**, 687 (2007).
- [51] P. Giannozzi, O. Andreussi, T. Brumme, O. Bunau, M. B. Nardelli, M. Calandra, R. Car, C. Cavazzoni, D. Ceresoli, M. Cococcioni *et al.*, *J. Phys.: Condens. Matter* **29**, 465901 (2017).
- [52] A. A. Mostofi, J. R. Yates, G. Pizzi, Y. S. Lee, I. Souza, D. Vanderbilt, and N. Marzari, *Comput. Phys. Commun.* **185**, 2309 (2014).
- [53] Defected atoms are the selected two atoms (bond) and their four surroundings. The ratio of defected atoms is defined as $(2 + 4)/2N$, in which 2 and 4 denote the selected two atoms and the four surroundings, respectively. $2N$ is the total atoms number in the cell. For example, the ratios for SW-graphene with size of $\sqrt{8}$ and $\sqrt{32}$ are $6/16$ and $6/64$, respectively.